Analytical Study of the Subsonic Wing-Rock Phenomenon for Slender Delta Wings

A. H. Nayfeh,* J. M. Elzebda,† and D. T. Mook‡
Virginia Polytechnic Institute and State University, Blacksburg, Virginia

An analytic expression describing the aerodynamic roll moment has been obtained from the numerical simulation of wing rock. This expression is used in the equation governing the rolling motion of a delta wing around its midspan axis. The result is used to construct phase planes, which reveal the general global nature of wing rock—stable limit cycles, unstable foci, saddle points, and domains of initial conditions leading to oscillatory motion and divergence. An asymptotic approximation to the solution of the governing equation is obtained; this result provides expressions for the amplitudes and frequencies of limit cycles. The present analysis provides a penetrating global view of the wing-rock phenomenon.

Introduction

In 1981 and 1982, respectively, wind-tunnel experiments were conducted using delta wings of aspect ratio 0.705 mounted on free-to-roll stings.[1,2] In both studies, the wings were placed in a steady airstream and the angle of attack was increased until rolling developed spontaneously. The arrangement is depicted in Fig. 1. Nguyen et al.[1] placed the axis of rotation below the centerline of the wing ($d \neq 0$). Levin and Katz placed the axis of rotation on the centerline ($d = 0$), housing the bearing assembly inside a fuselage-like tube. In 1983, after considering the data, Ericsson[3] concluded that wing rock is caused by the symmetric arrangement of the leading-edge-vortex system becoming unstable, never by vortex breakdown when the leading-edge sweep is more than 74 deg.

Later, Konstadinopoulos,[4] Konstadinopoulos et al.,[5] and Mook and Nayfeh[6] developed a numerical simulation of these wind-tunnel experiments. In their simulations, the equations governing the motion of the wing were integrated numerically. The general unsteady vortex-lattice method was used to predict the aerodynamic loads. There is a complication with this approach: the equations of motion cannot be integrated unless the loads are known, and the loads cannot be calculated unless the motion is known. To break this impasse, Konstadinopoulos et al.[5] developed an iteration scheme based on the predictor-corrector method. The resulting algorithm integrates forward in time, iterating at each time step until loads and motion are consistent. The results predict both simultaneously and interactively the motion of the wing and the flowfield. The prediction of the flowfield includes the wake where the history of the motion resides. The model simulates hysteresis, aerodynamic damping, and leading-edge separation. It is not limited by angle of attack, twist, camber, or planform as long as vortex bursting does not occur in the near vicinity of the wing.

The numerical simulation predicts onset angles and the periods and amplitudes of the ensuing limit cycles in close agreement with those from the first two sets of experiments. Moreover, the simulation shows that the symmetric arrangement of the leading-edge-vortex system at zero roll becomes unstable. The asymmetry causes a roll moment to develop. But as the angle of roll increases, the change in the apparent direction of the freestream causes the direction of the moment and, eventually, the direction of rotation to change.

Received Nov. 19, 1987; revision received July 20, 1988.

*Engineer, Aerodynamics Division.
†Engineer, Propulsion Engineering Division.
‡Professor, Engineering Mechanics Division.

Because the simulation provides the loads as functions of time, it is possible to develop an analytic expression for the roll moment.[4,5] The result is a third-order polynomial in roll angle and roll rate that fits the numerical data extremely well from the start of the motion through the development of limit cycles or decay, depending on the angle of attack. In the present paper, we substitute this expression into the equation of motion and obtain phase planes and approximate solutions using the method of multiple scales. The results provide a useful new analytic simulation of the experiments. The present paper describes a general approach that could be applied to other similar problems after an analytic expression for the loads has been found. Of course, the accuracy of the analytic results are limited by the accuracy of the expression for the loads.

The Problem

We consider a uniform, flat, thin wing, supported on a free-to-roll sting as shown in Fig. 1. The equation of motion is

$$\ddot{\phi} = c_1 c_l - c_2 \dot{\phi} \tag{1}$$

where ϕ is the roll angle, c_l is the aerodynamic roll-moment coefficient supplied by the unsteady-vortex-lattice method, and

$$c_1 = \rho S c L_c^2 / 2 I_{xx} \tag{2}$$

$$c_2 = \mu_x L_c / I_{xx} U_c \tag{3}$$

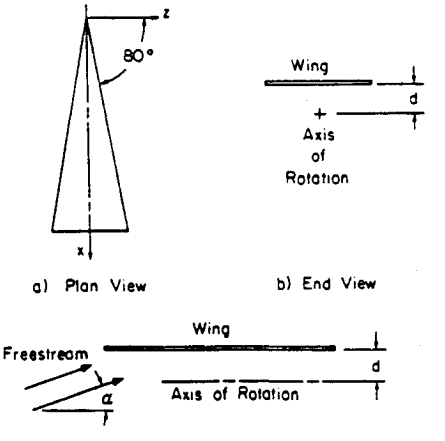

Fig. 1 Schematic representation of a delta wing on a free-to-roll sting: $d \neq 0$ corresponds to the experiments of Nguyen et al. and $d = 0$ corresponds to the experiments of Levin and Katz.

where ρ is the density of the air, S the area of the planform, c the chord, L the characteristic length, I_{xx}^c the moment of inertia with respect to the midspan axis along the chord, μ_x the damping coefficient for the sting bearing, and U_c the characteristic speed. The dot in Eq. (1) implies the derivative with respect to the nondimensional time

$$t^* = (U_c/L_c)t \tag{4}$$

In Refs. 4 and 5, solutions of Eq. (1) were obtained numerically. The general unsteady vortex-lattice method was used to predict the loads, and the numerical integration was accomplished by a modification of the predictor-corrector method. That solution predicts both the motion of the wing and of the fluid simultaneously, fully accounting for dynamic/aerodynamic interaction. The predicted results for onset angle (i.e., the lowest angle of attack for which rolling develops spontaneously) and amplitudes and periods of the ensuing limit cycles agree very well with the observations in Refs. 1 and 2. Here we provide an analytical solution. To obtain such a solution, one must have analytic expression for c_l. Such an expression is obtained next.

It is convenient to use a specific example to explain the procedure. We choose the following delta wing:

Leading-edge-sweep angle = 80 deg
Aspect ratio = 0.705
Chord = 0.429 m
L_c = chord/4
Area = 0.0324 m^2
Mass = 0.284 kg
$I_{xx} = 0.27 \times 10^{-3}$ kg-m^2

This is the same wing used by Levin and Katz.[2] In addition, we choose $\rho_{air} = 0.12 \times 10^{-2}$ kg/m^3 and $U_c = 15$ m/s. These values for the density and speed of the airstream agree with the test conditions in the experiments of Levin and Katz. Finally, we choose the damping coefficient for the bearing in the sting to be $\mu_x = 0.378 \times 10^{-4}$ kg-m^4/s. All of the numerical results were obtained using only this one value of μ_x; this value was found by trial and error to be the only value for which onset angle, period, and amplitude agree with experiment. These choices lead to $c_1 = 0.354$ and $c_2 = 0.001$.

One can readily fit a polynomial to the roll-moment calculated in the numerical simulation; it was found that the following gives virtually perfect agreement:

$$c_l = a_1\phi + a_2\dot{\phi} + a_3\phi^3 + a_4\phi^2\dot{\phi} + a_5\phi\dot{\phi}^2 \tag{5}$$

The values of the a_i depend on the angle of attack; they are given in Table 1. In Fig. 2, both the calculated moment and the moment given by Eq. (5) are shown as functions of time for two angles of attack, one stable (Fig. 2a) and one unstable (Fig. 2b). Equation (5) fits the calculated moment through the transients and into the regime where steady-state motion exists.

The form for c_l as given in Eq. (5) evolved from a much more general beginning, which included a total 12 terms in a fifth-order polynomial. Seven of the terms were sytematically eliminated because their contributions were small. The general form recognized that certain symmetries must exist; e.g., a constant would remove $\phi = 0$ from the equilibrium points, and even powers of ϕ would show the moment to be biased in one direction.

Table 1. Coefficients in the analytical expression for the roll moment, Eq. (5), at different angles of attack

α	a_1	a_2	a_3	a_4	a_5
15	−0.01026	−0.02117	−0.14181	0.99735	−0.83478
21.5	−0.04207	0.01456	0.04714	−0.18583	0.24234
22.5	−0.04681	0.01966	0.05671	−0.22691	0.59065
25	−0.05686	0.03254	0.07334	−0.3597	1.4681

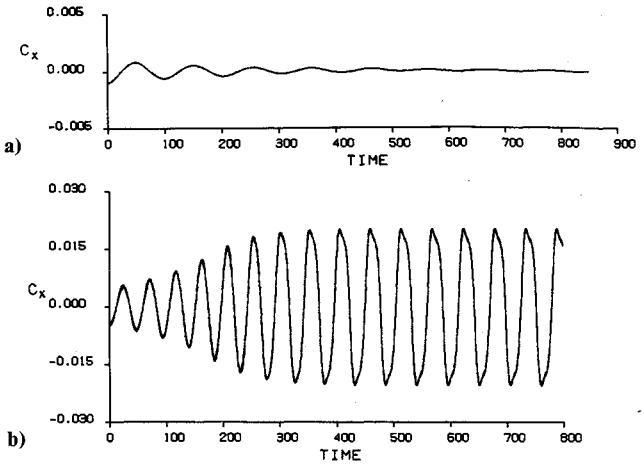

Fig. 2 Roll-moment coefficients as a function of time for $\alpha = 15$ deg (a stable case), and $\alpha = 25$ deg (an unstable case). Each plot contains the value of c_x from the numerical simulation and the value from Eq. (5). The results are virtually identical.

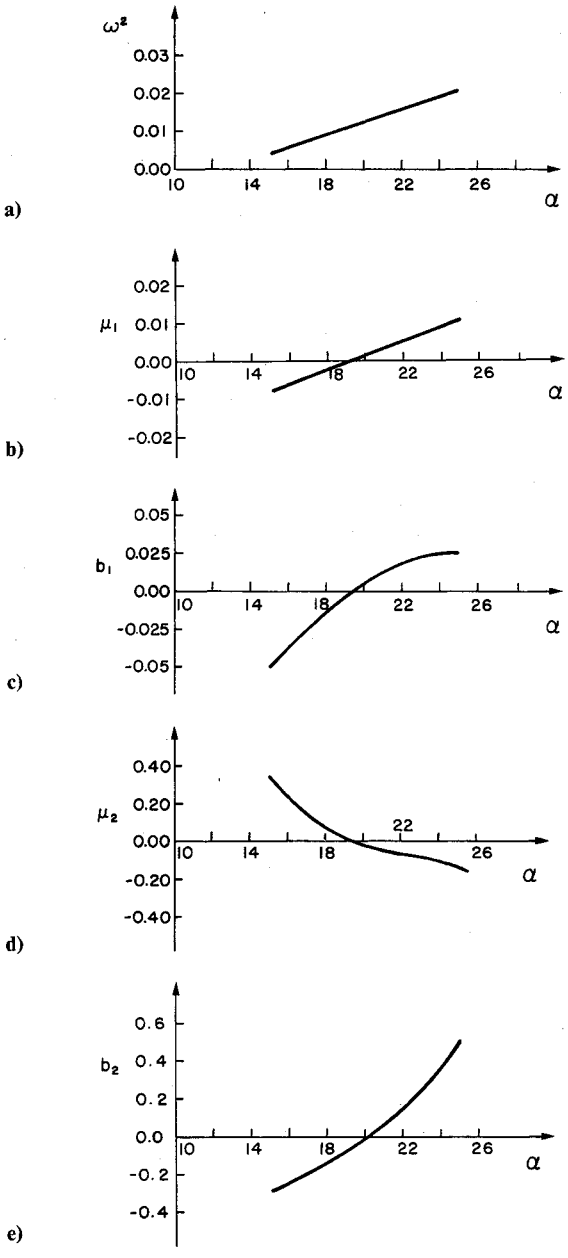

Fig. 3 The coefficients in Eq. (6) as functions of the angle of attack.

Substituting Eq. (5) into Eq. (1) leads to

$$\ddot{\phi} + \omega^2\phi = \mu_1\dot{\phi} + b_1\dot{\phi}^3 + \mu_2\phi^2\dot{\phi} + b_2\phi\dot{\phi}^2 \tag{6}$$

where

$$\omega^2 = -c_1a_1$$
$$\mu_1 = c_1a_2 - c_2$$
$$b_1 = c_1a_3$$
$$\mu_2 = c_1a_4$$
$$b_2 = c_1a_5$$

The coefficients in Eq. (6) are plotted as functions of angle of attack in Fig. 3. The point where μ_1 is zero corresponds to the onset of wing rock; the observed onset angle[2] is "19–20 deg." The values of the coefficients can be found for any angle of attack from these graphs.

Analysis

To analyze Eq. (6), we first construct phase planes for different angles of attack. Then, we obtain the motion in the neighborhoods of the various equilibrium positions. Finally, we analyze the limit-cycle motion.

Phase Planes

We begin by rewriting Eq. (6) as a system of two first-order equations:

$$\dot{\phi} = \dot{Y}_1 = \dot{Y}_2 \tag{7a}$$

$$\ddot{\phi} = \dot{Y}_2 = -\omega^2Y_1 + \mu_1Y_2 + b_1Y_1^3 + \mu_2Y_1^2Y_2 + b_2Y_1Y_2^2 \tag{7b}$$

To find the equilibrium (fixed) positions, we put

$$\dot{Y}_1 = \dot{Y}_2 = 0 \tag{8}$$

It then follows that

$$Y_1 = 0, \pm\omega/\sqrt{b_1} \tag{9}$$

The nonzero solution exists only when b_1 is greater than zero. Referring to Fig. 3, we see that b_1 and μ_1 change sign at the same angle of attack. At the angle of attack when b_1 is zero, two of these equilibrium positions are at infinity. As the angle of attack increases, these two point move toward the origin.

To determine the character of the motion in a small neighborhood of these equilibrium positions, we introduce the following change in variables (see, e.g., Chap. 3 of Ref. 7):

$$Y_1 = Y_{10} + u_1 \tag{10a}$$

$$Y_2 = u_2 \tag{10b}$$

where Y_{10} is the coordinate of an equlibrium position ($Y_{20} = 0$ at all equilibrium points). Substituting Eqs. (10) into Eqs. (7) and retaining only linear terms in u_1 and u_2 in the result, one finds the following:

$$\dot{u}_1 = u_2 \tag{11a}$$

$$\dot{u}_2 = (3b_1Y_{10}^2 - \omega^2)u_1 + (\mu_1 + \mu_2Y_{10}^2)u_2 \tag{11b}$$

This set of linear equations with constant coefficients has a solution in the form

$$(u_1,u_2) = (c_1,c_2)\exp(\lambda t) \tag{12}$$

where in general the eigenvalues are given by

$$\lambda = \tfrac{1}{2}\{\mu_1 + \mu_2Y_{10}^2 \pm [12b_1Y_{10}^2 - 4\omega^2 + (\mu_1 + \mu_2Y_{10}^2)^2]^{1/2}\} \tag{13}$$

At the origin ($Y_{10} = 0$), Eq. (13) reduces to

$$\lambda = \tfrac{1}{2}\{\mu_1 \pm i[4\omega^2 - \mu_1^2]^{1/2}\} \tag{14}$$

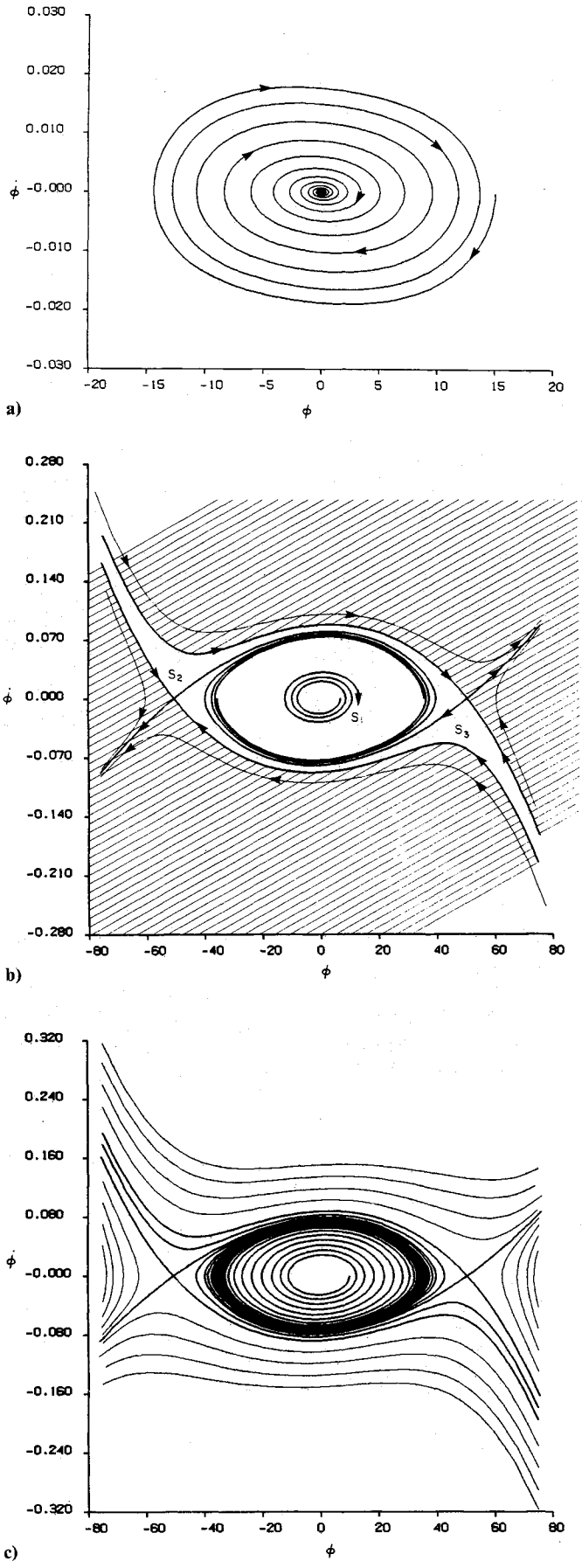

Fig. 4 Phase planes obtained by numerical integration of Eq. (6): a) $\alpha = 15$ deg; b) $\alpha = 25$ deg (the trajectories initiated in the shaded region diverge, and all the others approach the stable limit cycle); and c) many trajectories for the case $\alpha = 25$ deg.

Using the results in Fig. 3, one finds that $4\omega^2 > \mu_1^2$ for the range of angle of attack considered here (15 deg $\leq \alpha \leq$ 25 deg). Hence, the origin is a stable focus for $\alpha < 19.5$ deg approximately, and an unstable focus otherwise. The transition from stability to instability of the origin conicides with the appearance of two additional equilibrium points and with the onset angle of attack observed by Levin and Katz.[2] Next, we determine the character of the motion in a small neighborhood of the nonzero equilibrium points.

Using the results given in Eq. (9), one finds that for the equilibrium positions away from the origin

$$\lambda = \frac{1}{2}\left\{\mu_1 + \frac{\mu_2\omega^2}{b_1} \pm \left[8\omega^2 + \left(\mu_1 + \frac{\mu_2\omega^2}{b_1}\right)^2\right]^{1/2}\right\} \tag{15}$$

It follows that regardless of the sign of $\mu_1 + \mu_2\omega^2/b_1$, both eigenvalues are real; one is positive and the other is negative. Thus, whenever nonzero equilibrium points exist they are always saddle points.

These results are summarized in Fig. 4 where the entire phase planes for $\alpha = 15$ deg (Fig. 4a) and $\alpha = 25$ deg (Fig. 4b) are shown. These planes were constructed by numerically integrating Eqs. (7). For $\alpha = 15$ deg, the only equilibrium position is the origin ($b_1 < 0$), and it is stable. For $\alpha = 25$ deg, there are three equilibrium positions; using the results in Fig. 3, one finds that they are

$$Y_{10} = 0, \pm 50.45 \text{ deg} \tag{16}$$

Any motion initiated at a point in the shaded region of Fig. 4b will diverge, not oscillate; that is, the wing will continuously execute complete revolutions. The numerical simulation presented in Refs. 4 and 5 also predicts divergence. Any motion initiated at a point in the unshaded region will converge onto the limit cycle; that is, small-amplitude initial conditions lead to motions that grow to the stable limit cycle and large-amplitude initial conditions in the unshaded region lead to motions that decay to the limit cycle. Figure 4c shows the trajectories for many different initial conditions. Next, we obtain an asymptotic approximation to the solution of Eq. (6) and determine formulas for the amplitude and period of the limit cycle.

Asymptotic Approximation of Limit-Cycle Motion

Here we use the method of multiple scales[7-9] to construct an approximation to the solution of Eq. (6) that is valid for small, but finite, amplitudes of the motion. We begin by putting

$$\phi \simeq \epsilon^{1/2}u_1(T_0,T_1) + \epsilon^{3/2}u_2(T_0,T_1) \tag{17}$$

Here ϵ serves as a measure of the amplitude of the motion ($\epsilon \ll 1$), and

$$T_n = \epsilon^n t \tag{18}$$

There is no ϵ appearing naturally in the statement of this problem; ϵ is artificial and can be viewed as a bookkeeping tool. As we shall see, there will be no ϵ in the final result.

Using the chain rule, one finds that derivatives with respect to t become expansions in terms of partial derivatives with respect to the fast and slow scales (T_0 and T_1, respectively):

$$\frac{d}{dt} = D_0 + \epsilon D_1 \tag{19a}$$

$$\frac{d^2}{dt^2} = D_0^2 + 2\epsilon D_0 D_1 \tag{19b}$$

where

$$D_n = \frac{\partial}{\partial T_n} \tag{19c}$$

Substituting Eqs. (17) and (19) into Eq. (6), and then setting the coefficients of each power of ϵ equal to zero independently, one obtains the following:

$$D_0^2u_1 + \omega^2u_1 = 0 \tag{20}$$

$$D_0^2u_2 + \omega^2u_2 = -2D_0D_1u_1 + \hat{\mu}_1D_0u_1 + b_1u_1^3 + \mu_2u_1^2D_0u_1 + b_2u_1(D_0u_1)^2 \tag{21}$$

In order to arrive at these equations, one must put $\epsilon\hat{\mu}_1 = \mu_1$. This step forces the damping and nonlinearity to interact and, consequently, is essential.[7,9] Subsequently, we shall return to the original variables and parameters when we express the final result.

The solution of Eq. (20) can be expressed as

$$u_1 = a\cos(\omega T_0 + \beta) \tag{22}$$

Equation (20) is a partial differential equation (in the fast scale T_0); consequently, both a and β are functions of the slow scale T_1, not constants. It is convenient to use complex variables, so that we rewrite Eq. (22) as

$$\begin{aligned} u_1 &= \tfrac{1}{2}a\{\exp[i(\omega T_0 + \beta)] + \exp[-i(\omega T_0 + \beta)]\} \\ &= \tfrac{1}{2}a\exp(i\beta)\exp(i\omega T_0) + cc \\ &= A\exp(i\omega T_0) + cc \end{aligned} \tag{23}$$

where cc denotes the complex conjugate of the preceding terms and

$$A(T_1) = \tfrac{1}{2}a\exp(i\beta) \tag{24}$$

At this point, A is an arbitrary function of T_1. Subsequently, we shall choose A in such a way that renders the approximation uniformly valid as t (and hence T_0) becomes large.

Next, we substitute Eq. (23) into Eq. (21) and collect terms:

$$D_0^2u_2 + \omega^2u_2 = [-i\omega(2D_1A - \hat{\mu}_1A) + (3b_1 + \omega^2b_2 + i\omega\mu_2)A^2\bar{A}]\exp(i\omega T_0) + (b_1 - \omega^2b_2 + i\omega\mu_2)A^3\exp(3i\omega T_0) + cc \tag{25}$$

In order to eliminate secular terms (i.e., terms proportional to the factor $T_0\exp(i\omega T_0)$§ from u_2, we must put

$$i\omega(2D_1A - \hat{\mu}_1A) - (3b_1 + \omega^2b_2 + i\omega\mu_2)A^2\bar{A} = 0 \tag{26}$$

Substituting Eq. (24) into Eq. (26), then separating the result into real and imaginary parts, and returning to the original time scale and coefficients, we obtain

$$\frac{d\tilde{a}}{dt} = \frac{\mu_1\tilde{a}}{2} + \frac{\mu_2}{8}\tilde{a}^3 \tag{27}$$

$$\frac{d\beta}{dt} = -\left(\frac{3b_1 + \omega^2b_2}{8\omega}\right)\tilde{a}^2 \tag{28}$$

where $\tilde{a} = \epsilon^{1/2}a$ and it is implied that $\tilde{a} \neq 0$. Equation (27) can be solved for $\tilde{a}$, and the result can then be used to obtain β

§If u_2 contains this factor, then $|u_2|/|u_1|$ will grow without bound as t approaches inifinity. Such an expansion is useful over a limited time. Here we seek the expansion for which $|u_2|/|u_1|$ remains bounded.

Table 2 Amplitudes and periods (T) of the limit cycles and positions of the saddle points for different angles of attack

α	Amplitude: Numerical simulation	Amplitude: Analytical model	$T\omega/2\pi$	Y_{10}
15	—	—	—	—
21.5	28.28	28.79	1.11	±54.12
22.5	31.52	31.49	1.15	±52.06
25	33.14	32.94	1.18	±50.45

from Eq. (28). The results are

$$\tilde{a} = 2\left[\frac{\mu_1}{K\exp(-\mu_1 t) - \mu_2}\right]^{1/2} \tag{29}$$

$$\beta = \beta_0 + \left(\frac{3b_1 + \omega^2 b_2}{2\omega\mu_2}\right) \ln\left(\frac{K - \mu_2 \exp(\mu_1 t)}{K - \mu_2}\right) \tag{30}$$

where

$$K = \frac{4\mu_1 + \mu_2 \tilde{a}_0^2}{\tilde{a}_0^2} \tag{31}$$

in which $\tilde{a}_0$ is the initial amplitude and β_0 is the initial phase.

Substituting these results into Eqs. (22) and (17), we find that the first approximation to the solution of Eq. (6) is

$$\phi \simeq 2\left[\frac{\mu_1}{K\exp(-\mu_1 t) - \mu_2}\right]^{1/2} \cos(\omega t + \beta) \tag{32}$$

where β and K are given by Eqs. (30) and (31), respectively. It should be noted that ϵ does not appear in the final result; the $\tilde{a}_0$ represents the actual value of the initial amplitude.

It follows from Eq. (32) that, if μ_1 is less than zero, ϕ decays approximately in proportion to $\exp(\frac{1}{2}\mu_1 t)$, similar to the behavior of a linear damped oscillator. On the other hand, if μ_1 is greater than zero,

$$\phi \to 2\left(\frac{\mu_1}{-\mu_2}\right)^{1/2} \cos(\omega t + \beta) \tag{33}$$

as $t \to \infty$. The amplitude of the long-time motion is independent of the initial conditions; this is the amplitude of the limit cycle shown in Figs. 4b and 4c. When a limit cycle develops, it follows from Eq. (28) that the frequency is approximately given by

$$\frac{d}{dt}(\omega t + \beta) = \omega + \mu_1(3b_1 + \omega^2 b_2)/2\mu_2\omega \tag{34}$$

It follows that the period is

$$T \simeq \frac{2\pi}{\omega + [\mu_1(3b_1 + \omega^2 b_2)/2\mu_2\omega]} \tag{35a}$$

$$\simeq \frac{2\pi}{\omega}\left[1 - \mu_1(3b_1 + \omega^2 b_2)/2\mu_2\omega^2\right] \tag{35b}$$

Finally, we note that the limit-cycle amplitude can be obtained directly from Eq. (27) by setting $d\tilde{a}/dt = 0$, and the corresponding value of $d\beta/dt$ can be obtained directly from Eq. (28).

The results are summarized in Table 2 where the amplitude and period of the limit cycles and the positions of the saddle points are given as functions of angle of attack. As the angle of attack increases, the amplitude and period also increase. For angles of attack greater than 27 deg, the numerical simulation no longer agrees well with the observations. The difference is most likely the result of vortex bursting, a phenomenon that is not modeled by the numerical simulation and hence not described by the present expression for the moment.

Concluding Remarks

Earlier numerical simulations of the subsonic wing-rock phenomenon for slender delta wings, which agreed closely with wind-tunnel experiments, provided the roll moment as a function of time. These numerical data can be accurately fit by a five-term, third-order polynomial in roll angle and roll rate. In the present paper, this polynomial is used to construct phase planes that show the locations of equilibrium positions, limit cycles, and domains of initial conditions that lead to the different possible motions. In addition, the use of this polynomial in the equation of motion makes it possible to obtain asymptotic approximations to the expressions for limit-cycle amplitudes and periods. The asymptotic results are in close agreement with numerical solutions of the equation of motion based on the polynomial expression for roll moment, which in turn are in close agreement with the numerical simulations and wind-tunnel observations. The present analysis provides another view of the wing-rock phenomenon.

Acknowledgment

This work was sponsored by the Air Force Office of Scientific Research under Grant AFOSR-85-0158.

References

[1]Nguyen, L. T., Yip, L., and Chambers, X., Jr., "Self-Induced Wing Rock of Slender Delta Wings," AIAA Paper 81-1883, Aug. 1981.

[2]Levin, D. and Katz, J., "Dynamic Load Measurements with Delta Wings Undergoing Self-Induced Roll-Oscillations," *Journal of Aircraft*, Vol. 21, Jan. 1984, pp. 30–36.

[3]Ericsson, L. E., "The Fluid Mechanics of Slender Wing Rock," *Journal of Aircraft*, Vol. 21, May 1984, pp. 322–328.

[4]Konstadinopoulos, P. A., "Numerical Simulation of the Subsonic Wing-Rock Phenomenon," Ph.D. Thesis, Dept. of Engineering Mechanics, Virginia Polytechnic Inst. and State Univ., Blacksburg, VA, 1984.

[5]Konstadinopoulos, P., Mook, D. T., and Nayfeh, A. H., "Subsonic Wing Rock of Slender Delta Wings," *Journal of Aircraft*, Vol. 22, March 1985, pp. 223–228.

[6]Mook, D. T. and Nayfeh, A. H., "Application of the Vortex-Lattic Method on High-Angle-of-Attack Subsonic Aerodynamics," Society of Automotive Engineers Paper 851817, 1985.

[7]Nayfeh, A. H. and Mook, D. T., *Nonlinear Oscillations*, Wiley-Interscience, New York, 1979.

[8]Nayfeh, A. H., *Perturbation Methods*, Wiley-Interscience, New York, 1973.

[9]Nayfeh, A. H., *Introduction to Perturbation Techniques*, Wiley-Interscience, New York, 1981.